TECHNICAL NOTE OPEN ACCESS

Nanoscopic Profiling of Small Extracellular Vesicles via High-Speed Atomic Force Microscopy (HS-AFM) Videography

Muhammad Isman Sandira[1,2] | Keesiang Lim[1] | Takeshi Yoshida[1,3] | Elma Sakinatus Sajidah[1] | Shinnosuke Narimatsu[1,2] | Reon Imakawa[4] | Kota Yoshimura[4] | Goro Nishide[1,5] | Yujia Qiu[1,2] | Azuma Taoka[1] | Masaharu Hazawa[1,6] | Toshio Ando[1] | Rikinari Hanayama[1,3] | Richard W. Wong[1,2,5,6]

[1]WPI-Nano Life Science Institute, Kanazawa University, Kanazawa, Ishikawa, Japan | [2]Division of Nano Life Science in the Graduate School of Frontier Science Initiative, Kanazawa University, Kanazawa, Ishikawa, Japan | [3]Department of Immunology, Graduate School of Medical Sciences, Kanazawa University, Kanazawa, Ishikawa, Japan | [4]The School of Biological Science and Technology, College of Science and Technology, Kanazawa University, Kanazawa, Ishikawa, Japan | [5]Division of Nano Life Science in the Graduate School of Frontier Science Initiative, WISE Program for Nano-Precision Medicine, Science and Technology, Kanazawa University, Kanazawa, Ishikawa, Japan | [6]Cell-Bionomics Research Unit, Institute for Frontier Science Initiative (INFINITI), Kanazawa University, Kanazawa, Ishikawa, Japan

Correspondence: Keesiang Lim (limkeesiang@staff.kanazawa-u.ac.jp) | Richard W. Wong (rwong@staff.kanazawa-u.ac.jp)

ABSTRACT

Small extracellular vesicles (sEVs), which carry lipids, proteins and RNAs from their parent cells, serve as biomarkers for specific cell types and biological states. These vesicles, including exosomes and microvesicles, facilitate intercellular communication by transferring cellular components between cells. Current methods, such as ultracentrifugation and Tim-4 affinity method, yield high-purity sEVs. However, despite their small size, purified sEVs remain heterogeneous due to their varied intracellular origins. In this technical note, we used high-speed atomic force microscopy (HS-AFM) in conjunction with exosome markers (IgG^{CD63} and IgG^{CD81}) to explore the intracellular origins of sEVs at single-sEV resolution. Our results first revealed the nanotopology of HEK293T-derived sEVs under physiological conditions. Larger sEVs (diameter > 100 nm) exhibited greater height fluctuations compared to smaller sEVs (diameter ≤ 100 nm). Next, we found that mouse-origin IgG^{CD63}, and rabbit-origin IgG^{control} and IgG^{CD81}, exhibited the iconic 'Y' conformation, and similar structural dynamics properties. Last, exosome marker antibodies predominantly co-localised with sEV$_{d ≤ 100 nm}$ but not with sEV$_{d > 100 nm}$, demonstrating the CD63-CD81-enriched sEV and CD63-CD81-depleted sEV subpopulations. In summary, we demonstrate that nanoscopic profiling of surface exosome markers on sEVs using HS-AFM is feasible for characterising distinct sEV subpopulations in a heterogeneous sEV mixture.

1 | Introduction

Extracellular vesicles (EVs), first discovered by Chargaff and West in 1946 (Chargaff and West 1946) and later referred to as 'platelet dust' by Wolf in 1967 (Wolf 1967), are procoagulant particles originating from platelets found in normal plasma (Yáñez-Mó et al. 2015). Building on these foundational studies, EVs have since been isolated from a wide range of cell types and biological fluids, including saliva, urine, nasal and bronchial lavage fluid, amniotic fluid, breast milk, plasma, serum and seminal fluid (van Niel

et al. 2022). The MISEV2023 guideline provides a comprehensive overview of these different sources, underscoring the complexity and heterogeneity inherent in EV research (Welsh et al. 2024). This diversity poses significant challenges in obtaining consistent results for further analysis and applications (Kalluri and LeBleu 2020). EVs can be classified based on their cellular origin. Vesicles originating from multi-vesicular bodies (MVBs) are termed exosomes, whereas those generated from the plasma membrane are known as microvesicles/ectosomes. Emerging data indicate that the contents, dimensions and membrane compositions of EVs exhibit significant heterogeneity, influenced by intracellular origin, condition and external factors. Three primary subcategories of EVs have been identified: apoptotic bodies, cellular microparticles/microvesicles/ectosomes and exosomes (Yáñez-Mó et al. 2015). Exosomes are generally smaller, measuring around 40–160 nm in diameter, while ectosomes range from 50 to 1000 nm (Meldolesi 2018; van Niel et al. 2018). Exosomes and ectosomes of similar size could coexist in the purified sEV samples. However, universally recognised distinct markers to differentiate these categories are still lacking (Kalra et al. 2013; Tauro et al. 2012).

EVs transport a diverse array of substances, including proteins, lipids and nucleic acids such as DNA, mRNA, lncRNA, cirRNA and microRNA. Especially, these nucleic acids can be translated into functional proteins, thereby influencing the biological activities of recipient cells. The RNA content within EVs is of particular interest, with advanced RNA sequencing techniques revealing their regulatory roles in numerous biological processes and their potential as biomarkers for disease detection. They play a crucial role in intercellular communication, allowing cells to exchange information and materials (Nakajima and Tamai 2023). EV proteins primarily fall into two categories. The first group comprises structural and universally present proteins found on the surface or inside the cavity of EVs, including cytoskeletal elements, tetraspanin superfamily members (CD9, CD63, CD81, CD82), annexins, flotillin, Alix, TSG101 and heat shock proteins (HSP70 and HSP90). The second group is associated with the cellular source of EVs. For instance, EVs from antigen-presenting cells like macrophages and dendritic cells are rich in MHC-I and MHC-II molecules, while tumor cell-derived EVs may exhibit elevated levels of markers such as TGF-β and EpCAM (Wang et al. 2024). Recent studies have shown that small EVs containing transmembrane proteins such as chloride channel accessory 2 (CLCA2) (Seltmann et al. 2024) or androgen receptor (Read et al. 2017) can traverse the nuclear pore complex (Wong 2015), similar to the HIV capsid (Lim et al. 2024).

Proper EV preparation is essential for both fundamental research and clinical applications. The physicochemical properties of EVs often resemble those of lipoproteins and protein complexes, complicating the preparation process. Different preparation methods can affect the concentration and purity of EVs, impacting subsequent analyses. Therefore, selecting an appropriate preparation strategy is crucial to ensure research quality. Various techniques, including ultracentrifugation, density gradient centrifugation, size-exclusion chromatography, ultrafiltration, immunomagnetic separation, polymer precipitation, microfluidics platforms, asymmetric flow field-flow fractionation and anion exchange chromatography, each with their advantages and limitations (Kobayashi et al. 2024; Wang et al. 2024; Yoshida et al. 2024), have been developed for EV isolation. While current EV isolation techniques can reliably produce substantial yields, the precise characterisation of EV origin and purity remains a significant technical challenge. Identification of intracellular origins of EVs is the major research question as the biogenesis of EVs is highly heterogeneous. Nanoparticle tracking analysis (NTA) is limited to measuring the hydrodynamic diameters and concentrations of nanoparticles, lacking the ability to provide detailed structural information. Conversely, the use of western blotting to detect exosome markers is suboptimal for EV characterisation due to the inherent heterogeneity of the EV samples. Conceptually, like immune cells, immunophenotyping of EVs using surface markers could provide important clues regarding EV's intracellular origins. Nonetheless, due to the small size and low refractive index of EVs pose challenges to the resolution capabilities of standard flow cytometry. Although nano flow cytometry (NFC) has been developed (Kobayashi et al. 2024), fluorescent signals are still susceptible to interference from background noise (Yim et al. 2023).

Scanning probe microscopy (SPM) deploys a probe close to EV surface to elucidate its properties. Atomic force microscopy (AFM) imaging can be utilised to quantify the impact of EV preparation and isolation techniques on EV size distribution, shape and mechanical characteristics (Palanisamy et al. 2020; Parisse et al. 2017; Sharma et al. 2010; Yurtsever et al. 2021). Tapping mode AFM is a label-free, high-resolution technique that provides three-dimensional images of EV structures (Yurtsever et al. 2021). A higher temporal resolution version of AFM, the high-speed AFM (HS-AFM), is a distinctive method in dynamic structural biology that allows for the observation of individual molecules in motion (Ando et al. 2023; Umeda et al. 2023). This technique has been applied to investigate conformational dynamics of biomolecules (Nishide et al. 2021; Lim et al. 2023; Lim et al. 2021; Lim et al. 2020; Lim, Mohamed et al. 2020; Nishide et al. 2023), interactions between biomolecules (Nishide et al. 2021; Lim et al. 2023; Lim et al. 2021; Lim et al. 2020; Lim, Mohamed et al. 2020; Nishide et al. 2023), structural properties of organelles (Mohamed et al. 2020; Mohamed et al. 2017; Qiu et al. 2024; Sajidah et al. 2022), and interaction between biomolecules and organelles (Lim et al. 2023; Lim et al. 2020; Lim, Mohamed et al. 2020; Sajidah, Lim et al. 2024) at nanoscale resolution. Recently, HS-AFM videography has been used to identify dynamic IgG activities, such as walking on viral surfaces, oligomerisation and complement activation in response to antigen recognition (Lim et al. 2023; Preiner et al. 2014; Strasser et al. 2020; Strasser et al. 2019; Zhang et al. 2020).

In this technical note, we employed HS-AFM videography for nanoscopic profiling of surface exosome markers: the tetraspanin proteins CD63 and CD81, on individual sEV to differentiate between tetraspanin-enriched sEVs (exosome-like sEV) and tetraspanin-depleted sEV (ectosome-like sEV) isolated from HEK293T conditioned media. We demonstrate the initial step in the development of nanoscopic immunophenotyping of sEV, facilitating the creation of non-invasive, label-free detection techniques for sEV-based biomarkers, thereby enabling the early diagnosis of a range of diseases, including various cancers.

2 | Materials and Methods

2.1 | Cell Line and Antibodies

HEK293T cells were grown in Dulbecco's Modified Eagle's Medium (DMEM, Nacalai Tesque, Kyoto, Japan) supplemented with 10% fetal bovine serum (FBS; Life Technologies, CA, USA) and 1% Penicillin-Streptomycin (Nacalai Tesque, Kyoto, Japan). The cells were maintained at a temperature of 37°C in a humidified CO_2 incubator. Rabbit IgG control (FUJIFILM Wako Pure Chemical Corporation, catalog number: 148–09551), anti-human CD81 antibody (System Biosciences, catalog number: EXOAB-CD81A-1) and anti-human CD63 antibody (BioLegend, catalog number: 353039) were used for HS-AFM scanning in this study.

2.2 | sEVs Preparation, Purification and Characterisation

Extracellular vesicles (EVs) from the HEK293T cell line were isolated using the previously reported methodology (Lim et al. 2023; Lim et al. 2021; Sajidah et al. 2022). Following a 4-day culturing period, the cell-conditioned media was obtained and underwent differential centrifugation to exclude cells, debris and large EVs. Next, the supernatant above the sediment was passed through a 0.22-μm Millex-GV filter (Merck Millipore, MA, USA) to produce a purified cell conditioned medium called the 10K sup. Subsequently, the sEVs were purified from the 10K solution using a MagCapture Exosome Isolation Kit PS (Wako, Osaka, Japan) according to the instructions provided by the manufacturer. The isolated small extracellular vesicles (sEVs) were placed into a dialysis membrane with a molecular weight cut-off (MWCO) of 3500. They were then subjected to overnight dialysis in phosphate-buffered saline (PBS). The NanoSIGHT LM10 instrument, manufactured by Malvern Panalytical in Malvern, UK, was utilised to conduct nanoparticle tracking analysis (NTA) for the purpose of quantifying the content of sEVs. The purification method of sEV adheres to the MISEV2018 criteria (Théry et al. 2018) as we have previously submitted the protocol to the EV-TRACK knowledgebase in our earlier study (Lim et al. 2021) (EV-TRACK ID: EV210256).

2.3 | Nanofabrication of Cantilever Tip by Using Electron Beam Deposition (EBD)

An Olympus BL-AC10DS-A2 cantilever, manufactured in Tokyo, Japan, was utilised as a scanning probe for the purpose of scanning the sEVs. In water, the cantilever had a spring constant (k) of 0.1 N/m and a resonance frequency (f) of 0.6 MHz (1.5 MHz in air). The cantilever has dimensions of 9 μm (length), 2 μm (width) and 0.13 μm (thickness). The sensitivity of the tip-sample interaction can be influenced by the length of the cantilever tip. To resolve this problem, one can deposit amorphous carbon onto the cantilever tip using the EBD technique to extend the length of the cantilever tip, with an average length of 2.53 μm. Initially, the cantilever underwent a UV/O3 cleaning process, followed by immersion in a piranha solution comprising sulfuric acid and hydrogen peroxide. Subsequently, electron beam deposition (EBD) was performed on the cantilever using a field emission scanning electron microscope, ELS-7500 (Tokyo, Japan), with an accelerating voltage of 30-kV and an irradiation time of 2 min. An EBD-ed cantilever tip typically has a tip radius range of 6–8 nm.

2.4 | High-Speed Atomic Force Microscopy (HS-AFM) Imaging

The acquisition of HS-AFM images was performed using our laboratory-developed HS-AFM microscope, as previously stated (Mohamed et al. 2020; Mohamed et al. 2017). Briefly, a laser beam with a wavelength of 670 nm was directed through a 20× objective lens (CFI S Plan Fluor ELWD, Nikon, Tokyo, Japan) and concentrated on an EBD-ed cantilever tip. A two-segmented photodiode with position-sensing capability was utilised to detect the dynamic deflection of the cantilever. To ensure the integrity of the sample, it was necessary to provide a mild tapping force by setting the cantilever's free oscillation amplitude (A0) between 1.5 and 2.5 nm and the set point at 80%–90% of the free amplitude. A layer of muscovite mica, approximately 0.1 mm thick, was attached to a glass stage. The glass stage was then placed on an HS-AFM scanner. Next, poly-L-lysine (PLL)-coated mica substrate was prepared by treating the mica with 0.1% w/v PLL solution for 5 min and then washed twice with scanning buffer.

To capture the nanotopology of the sEVs, sEVs were loaded and incubated on the substrate for 10 min and then washed to remove the unbound sEVs. After that, the sEVs were scanned under a near-physiological buffer (50 mM Tris-HCl, 150 mM NaCl, pH 7.50) (Lim et al. 2023; Lim et al. 2021). To observe the real-time sEV interaction with antibodies, antibodies were added to sEVs that had adsorbed on the substrate, then incubated for 10 min, and eventually scanned using HS-AFM. In the premix setting, sEVs were incubated with antibodies overnight at 4°C and then proceeded to HS-AFM nanoimaging. Antibody dilutions for IgG control, anti-CD81 and anti-CD63 were 1:1000, 1:2500 and 1:5000, respectively. Experiments were repeated for a minimum of five times.

2.5 | Image Processing and Data Analysis of HS-AFM Data

The ImageJ program (https://imagej.nih.gov/ij/) was utilised to process and analyze all HS-AFM images. The HS-AFM images were initially processed using a fit polynomial filter with an order of 1 in both the x- and y-directions. This was followed by a low-pass filter, specifically a Gaussian blur, to reduce noise and improve the clarity of the images. The HS-AFM images were processed using the freeware Gwyddion to generate three-dimensional (3D) images. The spatial dimension analysis characteristics, such as height, diameter and area, were measured using Image J (Lim et al. 2020). Volumes of sEVs were computed by multiplying sEV area and cross-sectional height as reported previously (Sajidah et al. 2022). The processed image sequences were transformed into WMV format videos and subsequently modified and assembled using the Adobe Creative Cloud suite (https://www.adobe.com/creativecloud.html).

2.6 | Immunoblotting

HEK293T-derived sEVs were subjected to protein extraction using RIPA buffer. Protein concentration of sEV lysates were

determined with BCA protein assay kit (Thermo Fisher, MA, USA). EV lysates (50 μg/mL) were loaded onto an automated western blot system Wes (Bio-Techne, MN, USA) equipped with a 12–230 kDa separation module. EV markers (CD9, CD63, CD81, TSG101, HGS and VPS37B) and cellular marker (GAPDH) were detected using each primary antibody : anti-human CD9 antibody (clone HI9a, ×50, BioLegend), anti-human CD63 antibody (clone H5C6, ×50, BioLegend), anti-human CD81 antibody (clone 5A6, ×50, BioLegend), anti-TSG101 antibody (GTX118736, ×50, GENE-TEX), HGS antibody (C2C3), C-term (GTX101718, ×50, GENE-TEX), anti-VPS37B antibody (HPA038217, ×50, Atlas Antibody), nti-GAPDH mAb (clone 3H12, ×50, MBL), and corresponding HRP-conjugated secondary antibodies; HRP Goat anti-mouse IgG (minimal x-reactivity) antibody (405306, ×500, BioLegend) or HRP Donkey anti-rabbit IgG (minimal x-reactivity) antibody (406401, ×500, BioLegend).

2.7 | Statistical Analysis

The graphs for descriptive statistics were generated using Graph-Pad Prism version 7 (GraphPad, CA, USA). Statistical analysis was conducted using SPSS version 27 (IBM Group, NY, USA). The chi-square test was applied to determine the association between antibody co-localisation and diameter of sEV. Data normality was verified through the Kolmogorov-Smirnov or Shapiro-Wilk test, followed by the Spearman correlation test to determine variable relationships. Mann-Whitney U test was performed for comparative analysis. The level of statistical significance was set at $p < 0.05$, with a confidence range of 95%.

3 | Results

sEVs are valuable for studying biological and pathological processes, but their nanoscale size and low refractive index make visualisation challenging. Confocal microscopy can capture active sEV release sites, but it fails to detect sEVs due to the diffraction limit. While electron microscopy provides detailed images, sample fixation alters sEV native shapes. AFM and scanning ion-conductance microscopy (SICM) offer topographical imaging of sEVs in solution, yet their temporal resolution is limited. To direct observe sEVs with different sizes under HS-AFM, we first isolated high purity sEVs secreted by HEK293T cells using ultracentrifugation and Tim-4 affinity purification, as shown in Figure 1a. This method targets phosphatidylserine (PS) in the sEV membrane, with Tim-4 binding to PS in a Ca^{2+}-dependent manner. The presence of EDTA elutes intact sEVs from Tim-4 beads, thus overcoming the limitations of conventional affinity isolation and yielding highly pure heterogeneous sEVs. Our western blotting result showed that isolated sEVs expressed a set of exosomal markers including CD9, CD63, CD81, TSG101, HGS and VPS37B but not GAPDH (Figure S1a). Additionally, NTA analysis indicated most of the sEVs had size less than 200 nm (Figure S1b).

For direct visualisation, sEV samples were loaded on 0.1% PLL-coated mica and scanned using HS-AFM under a near-physiological condition (50 mM Tris HCl, 150 mM NaCl pH 7.5), as illustrated in Figure 1b. HS-AFM operates in amplitude modulation or 'tapping-mode', where the cantilever tip inter-mittently contacts the sample surface, reducing lateral friction and minimising EV surface deformation. Cantilever oscillation amplitude is detected via an optical-beam-deflection technique and maintained at a reference amplitude by a proportional-integral-derivative (PID) feedback controller. This setup keeps the interaction force constant, allowing for the construction of topographic images from PID signals (z-dimension) recorded at each pixel (x, y-dimensions). Standard AFM is commonly used to generate force curves for measuring the nano-mechanical properties of sEVs, such as stiffness (Figure 1c). The low temporal resolution of AFM hinders the observation of sEV structural dynamics as well as the dynamic interactions between sEVs and biomolecules (e.g., antibodies). In HS-AFM, the main objective is nanoimaging with high spatiotemporal resolution. Therefore, in contrast to standard AFM, a short cantilever with a high first resonance frequency in water is preferred for fast scanning. Cantilevers with high resonance frequency have lower noise density (Ando et al. 2007). Additionally, shorter cantilevers provide higher sensitivity in the optical beam deflection (OBD) detection of cantilever deflection (Ando et al. 2012). Our cantilevers, BL-AC10DS-A2 (Olympus), have short tips (typical tip height ~0.8 μm), which can affect scanning quality. To achieve ideal scanning quality, we perform electron beam deposition (EBD) using scanning electron microscopy to grow an amorphous carbon tip, lengthening the cantilever tip (Figure 1d). Last, a substrate with a flat and smooth surface is important for HS-AFM scanning. Muscovite mica is a suitable substrate that can easily be affixed to a glass stage (Figure 1e). Further functionalisation of mica is possible by coating it with poly-L-lysine, cations or other substances for specific sample adsorption. sEVs readily adsorbed onto 0.1% PLL-coated mica due to electrostatic interaction between the negatively charged phosphatidylserine (PS) lipid layer and positively charged PLL.

Spatial dimension analysis revealed heterogeneous sEV sizes. The kernel density plot, overlaid with a histogram of the sEV diameter distribution, revealed two distinct peaks in the sEV sample (Figure S1c). Using k-means clustering analysis, we identified two clusters of sEV had mean diameters of 66 and 119 nm, respectively. Generally, the size of exosome is 100 nm or less. Therefore, we separated the sEVs into two major groups: sEV with diameter lesser or equal to 100 nm ($sEV_{d \leq 100\,nm}$) and sEV with diameter greater than 100 nm ($sEV_{d > 100\,nm}$). The average height, diameter and volume of $sEV_{d > 100\,nm}$ were 43.98 ± 12.77 nm, 120 ± 16 nm, 4,80,029 ± 2,49,055 nm^3, respectively (Figures 2a). On the other hand, the average height, diameter, and volume of $sEV_{d \leq 100\,nm}$ were 28.79 ± 8.02 nm, 67 ± 14 nm and 1,08,799 ± 72,670 nm^3, respectively (Figures 2b). We measured the volume of sEV (Figure 2a,b) and then compared between $sEV_{d \leq 100\,nm}$ and $sEV_{d > 100\,nm}$ to account for surface distortion effect on sEV diameter. The results indicated that volume of $sEV_{d > 100\,nm}$ was significantly larger than that of $sEV_{d \leq 100\,nm}$ (Figure 2c). HS-AFM captured clear topographic images of both $sEV_{d \leq 100\,nm}$ and $sEV_{d > 100\,nm}$, demonstrating that sEVs are elastic spherical lipid sacs, with the sharp cantilever preserving the sEV structure. These results indicate HS-AFM's effectiveness in visualising sEVs with convoluted surfaces (Figure 2d, Figure S1d-f and Movie S1). In addition to 0.1% PLL, Ni^{2+}-coated mica is also suitable for sEV adsorption without causing rupture (Figure S2, Movie S2). Further
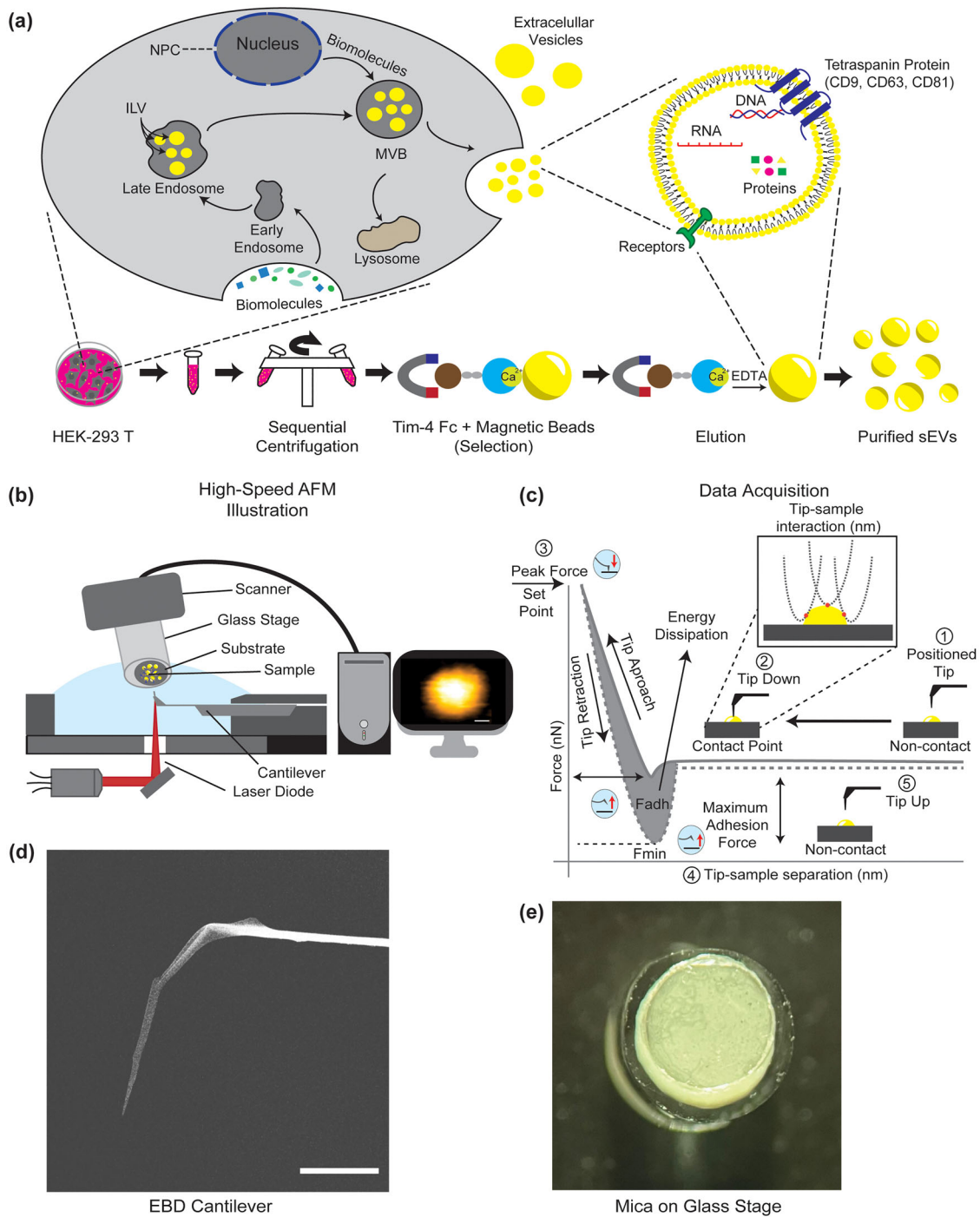
FIGURE 1 | Preparation of HEK293T-derived sEV for HS-AFM nanoimaging. (a) An illustration depicts the biogenesis and isolation of endosomal origin sEVs secreted by HEK293T cells using ultracentrifugation and Tim4 affinity method (ILV: intraluminal vesicles; MVB: multivesicular bodies; NPC: nuclear pore complex). (b) A schematic diagram illustrates the HS-AFM setup for nanoimaging of sEVs to visualise their nanotopology and interactions with antibodies. (c) A diagram presents the generation of force curve by conventional AFM used to characterise mechanical properties of sEVs. HS-AFM rather rely on optimal tip-sample interaction for nanoimaging without affecting sample integrity. (d) EBD lengthens cantilever tip length by growing an amorphous carbon tip on the existing tip (scale bar, 1 μm). The EBD-ed tip appears as the iconic 'bird-beak' appearance. (e) A flat and smooth mica substrate glued on a glass stage.

investigation of sequential playbacks revealed distinct dynamic behaviours among $sEV_{d \leq 100\,nm}$ and $sEV_{d > 100\,nm}$ (Figure 2e,f). We observed that $sEV_{d \leq 100\,nm}$ exhibited less height fluctuation compared to $sEV_{d > 100\,nm}$, suggesting increased membrane rigidity in $sEV_{d \leq 100\,nm}$ (Figure 2f). Taken together, these results indicate that HS-AFM is a feasible and effective tool for recording the native spatiotemporal dynamics of HEK293T-derived sEVs.
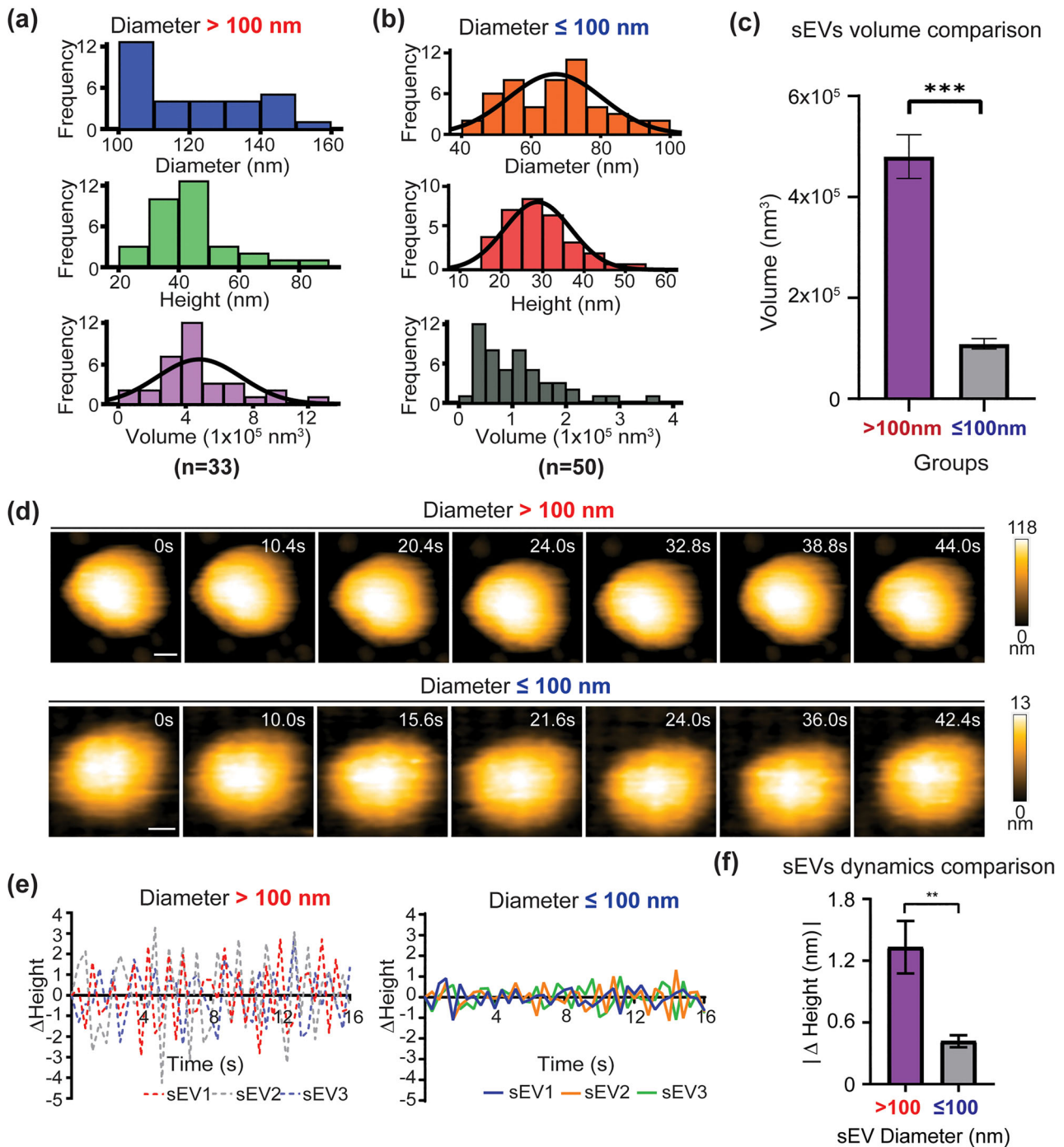
FIGURE 2 | HS-AFM nanoimaging of HEK293T-derived small extracellular vesicles. (a and b) Histograms with Gaussian distribution curves delineate the diameter, height, and volume, distributions of $sEV_{d>100\,nm}$ (a) and $sEV_{d\leq100\,nm}$ (b). (c) The volume of $sEV_{d>100\,nm}$ was significantly greater than that in $sEV_{d\leq100\,nm}$. Data are presented as mean $\pm$ S.E.M, *** $p < 0.001$ (n, sEV: 33; sEV: 50). (d) HS-AFM image sequence shows the direct real-time visualisation of $sEV_{d>100\,nm}$ and $sEV_{d\leq100\,nm}$ in a near-physiological buffer (scale bar, 50 nm). (e) Three representative line graphs of real-time height change are plotted separately for sEV with d > 100 nm and sEV with d ≤ 100 nm. (f) $sEV_{d>100\,nm}$ has a greater magnitude of height fluctuation compared with $sEV_{d\leq100\,nm}$ (n: 5; Two-tailed Student T test, ** $p < 0.01$).

Prior to nanoscopic profiling of sEVs using antibodies specific to exosome markers (CD63 and CD81), we performed HS-AFM nanoimaging of these antibodies. Since these antibodies are IgG, we first obtained the HS-AFM simulated image of a full-length mouse IgG1 crystal structure (PDB: 1IGY) using the bioAFMviewer (Amyot and Flechsig 2020), as shown in Figure

S3a. BioAFMviewer is a robust tool that generates high-quality HS-AFM-simulated images, providing reliable references for the HS-AFM community. The HS-AFM imaging of mouse-origin IgG[CD63] yielded structures closely resembling the IgG structure from the PDB data, clearly visualising the iconic 'Y' shape of IgG and differentiating the Fab (red and white arrows) and Fc (green
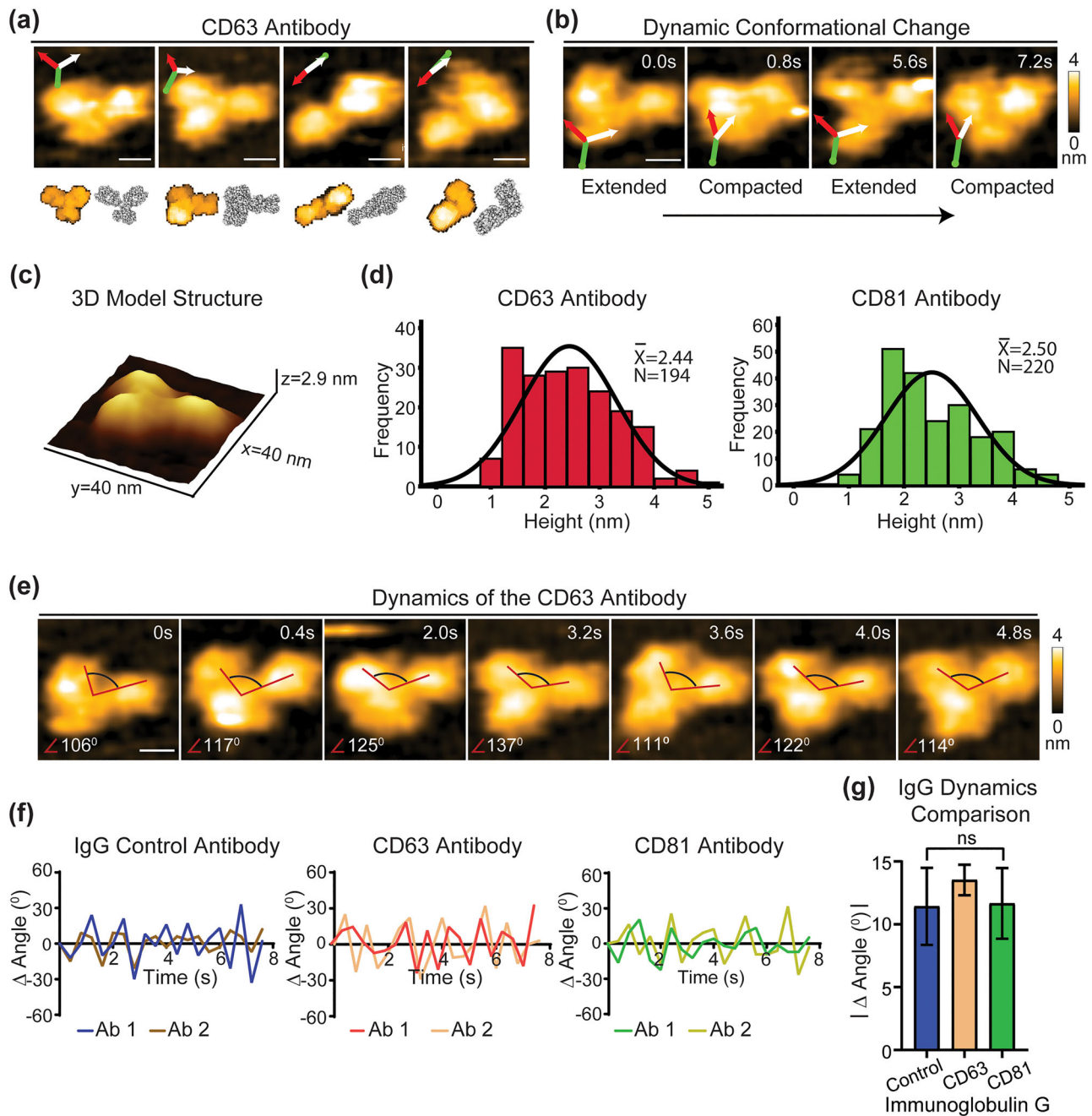
FIGURE 3 | Structural properties and molecular dynamics of IgG[control] and exosome marker antibodies. (a) HS-AFM image sequence displays the native conformation and conformational dynamics of IgG[CD63]. The antibody topology resembles the HS-AFM simulated image of IgG1 (PDB:1IGY) generated by the bioAFMviewer (bottom of each image). Fab and Fc regions are indicated by red/white arrows and a green arrow respectively (scale bar, 5 nm). (b) HS-AFM imaging revealed two interchangeable conformations of anti-CD63 antibody, the extended and compacted conformations, during scanning (scale bar, 5 nm). (c) 3D surface plot of an IgG[CD63]. (d) Two histograms with Gaussian distribution curves present the height distribution of IgG[CD63] and IgG[CD81]. (e) Rapid angular changes captured at millisecond level indicating the dynamic movement of Fab of IgG[CD63] (scale bar, 5 nm). (f) Two representative line graphs depict the angular changes of angle between two Fabs for IgG[control], IgG[CD63] and IgG[CD81], respectively. (g) No obvious difference in the magnitude of angular changes among these antibodies (n:3, one-way ANOVA, ns: not significant).

arrow) regions (Figure 3a,c, Movies S3 and S5). The dynamic movement of the two Fab regions observed during HS-AFM scanning resulted in the antibody exhibiting interchangeable extended and compacted conformations (Figure 3b, Movie S3). In the extended conformation, the two Fabs are widely separated, whereas in the compacted conformation, the two Fabs are in close proximity. This dynamic transition exhibited transient torsional

movements reminiscent of swinging arms (Figure 3b, Movie S3).

To achieve a predominantly monomeric state, antibodies were diluted. The cross-sectional height of IgG[CD63] was evaluated, and the average height ($n = 194$) was 2.44 nm (Figure 3d). Although both IgG[control] and IgG[CD81] are rabbit origin, they were

presented as Y-shape (Figure S3b,d, Movies S4 and S6) and possess a similar height profile to IgG^{CD63} (Figures 3d and S3c). The average height of IgG^{control} and IgG^{CD81} were 2.29 nm ($n = 225$) and 2.50 nm ($n = 220$), respectively (Figures 3d and S3c). Recognising the importance of IgG flexibility in binding affinity and avidity, we conducted an angle analysis on the Fab swivel movements, treating them as random walks. The estimated flexibility of the IgG hinge region was 116° (n for IgG^{control}, IgG^{CD63}, IgG^{CD81} = 2), aligning well with previous structural analyses of intact IgGs that indicated a Fab-Fab angle of approximately 110° in cryo-EM studies (Bongini et al. 2004) (Figures 3e,f and S3d, Movies S4–S6). The dynamic wagging motions were facilitated by the flexible hinge regions of IgG. We noticed that there was no significant difference in angular change among IgG^{control}, IgG^{CD81} and IgG^{CD63} (Figure 3g). This flexibility allows antibodies to maneuver in a fluid medium, effectively searching for antigens on surfaces, aiding in attachment, as well as Fc positioning for complement activation, phagocytosis and antibody-dependent cellular cytotoxicity (ADCC). These HS-AFM nanoscopic real-time videography data demonstrate that IgG^{CD63}, IgG^{CD81} and IgG^{control} can adopt flexible conformations, ranging from highly compact to fully extended, in response to varying epitope distances.

Next, we performed nanoscopic characterisation of sEVs using IgG^{CD63} and IgG^{CD81}. At the large scanning area, we observed sEVs with different sizes interacting with IgG^{CD63} and IgG^{CD81} but not IgG^{Control} (Figure S4). Real-time dynamic interaction between IgG^{CD63} or IgG^{CD81} and sEVs were filmed at high spatiotemporal resolution. The results showed that antibodies approached and interacted with sEVs. IgG^{CD63} or IgG^{CD81} contacted and bound steadily on sEV surface (Figure S5b,c, Movies S8 and S9). In contrast, IgG^{control} transiently bound and left the sEV surface, suggesting that antigen-antibody interaction but not non-specific interaction establish the steady bonding (Figure S5a, Movies S7). Importantly, these interactions did not alter the topological and spatial characteristics of the sEVs. To further reassure the antigen-antibody interaction, we incubated IgG^{CD63} or IgG^{CD81} with sEVs overnight at 4°C before HS-AFM scanning. We observed high co-localisation frequency of IgG^{CD63} and IgG^{CD81}, but not IgG^{control} with sEV$_{d \leq 100\,nm}$ (Figures 4a and S6a-c). Additionally, we found multiple IgG^{CD63} were co-localised with a single sEV.

Interestingly, the co-localisation frequency of IgG^{CD63} was significantly reduced in sEV$_{d > 100\,nm}$ (48%) compared to sEV$_{d \leq 100\,nm}$ (83%) (Figures 4a–c and S6a,d, Movie S10a,b). A similar trend was also observed in IgG^{CD81} (Figures 4a–c and S6b,d, Movie S10c,d). IgG^{control} exhibited minimal or nonspecific transient interaction with sEVs of any size (Figures 4a,b and S6c). Besides lateral interaction, we noticed a similar co-localisation pattern at the apical region of sEV (Figure S7, Movie S11). Further correlation analysis revealed a significant negative correlation between antibody co-localisation frequency and spatial parameters (height, diameter and volume) of sEVs (Figure 4d–f). A negative correlation was found stronger in IgG^{CD81} than in IgG^{CD63} (Figure 4d,e). This data suggests the presence of two distinct sEV subpopulations: CD63-CD81-enriched sEVs (exosome-like) and CD63-CD81-depleted EVs (MV/ectosome-like) in the purified sEV sample.

4 | Discussion

Extracellular vesicles (EVs), including exosomes, microvesicles/ectosomes, oncosomes and apoptotic bodies, play roles in physiological and pathological functions. Exosomes are crucial for studying cell-cell communication, disease pathogenesis and developing nanocarriers. Recently, exosomal biomarkers have shown clinical value in diagnosing and prognosing diseases, especially cancer. Despite robust isolation methods, ensuring pure exosome yields is challenging. Identifying the intracellular origin of EVs is difficult, as size alone is not a definitive parameter to distinguish exosomes from other EVs with equivalent size. For example, exosomes and ectosomes have distinct origins: exosomes are derived from endosomes, whereas ectosomes originate from the plasma membrane. Therefore, small extracellular vesicles (sEV) have been suggested as an appropriate term for exosomes to avoid confusion. Immunophenotyping of sEVs with specific surface markers using flow cytometry is an ideal approach for exosome characterisation. Nonetheless, the smaller size and low refractive index of sEVs limit the accuracy of flow cytometry. Furthermore, background noise in nanoflow cytometry can affect the instrument's performance.

In this study, we conducted HS-AFM nanoimaging to profile surface exosome markers expressed on sEV. We managed to differentiate a pool of sEV to tetraspanin-enriched sEVs (exosome-like sEV) and tetraspanin-depleted sEVs (ectosome-like sEV) using anti-CD63 and anti-CD81 antibodies. Understanding the intracellular origins of sEVs is pivotal for elucidating their formation mechanisms and their roles in various diseases. We isolated sEVs from HEK293T cells using ultracentrifugation and TIM4-affinity purification, followed by labeling with exosome markers antibodies. Although larger EVs could express tetraspanins, tetraspanin-enriched sEVs indicate exosomes with endosomal origin (Kowal et al. 2016). Unlike the conventional approaches (NTA or NFC), direct visualisation of sEV using HS-AFM enabled us to ignore minute sEV aggregates, ensuring the high accuracy of single sEV profiling. In addition, we could observe antibody docking to different sEV sizes, effectively distinguishing exosome marker-enriched subpopulations from depleted ones in a wide range of sample inputs, from pre-clinical to clinical samples. Real-time nanoscopic investigations revealed that both IgG^{CD63} and IgG^{CD81} preferentially co-localised with sEV$_{d \leq 100\,nm}$, but with minimal co-localisation with sEV$_{d > 100\,nm}$. Our results are supported by the findings reported by Zhang et al. (2018). First, they found that small exosomes (Exo-S; diameter: 60–80 nm) showed exosomal properties, whereas large exosomes (Exo-L; diameter: 90–120 nm) demonstrated ectosomal properties. Furthermore, CD63 was enriched in Exo-S but not in Exo-L. Second, they reported that Exo-S membrane was stiffer than the Exo-L membrane. Consistently, we demonstrated that sEV$_{d > 100\,nm}$ exhibited a greater magnitude of height fluctuation than sEV$_{d \leq 100\,nm}$. This suggests the existence of distinct sEV subpopulations in human cells that can be differentiated using HS-AFM nanoimaging techniques. By combining spatial analysis and surface exosome marker profiling, our results indicate that the CD63-CD81-enriched sEVs are likely to be the bona fide exosomes secreted by the HEK293T cells.
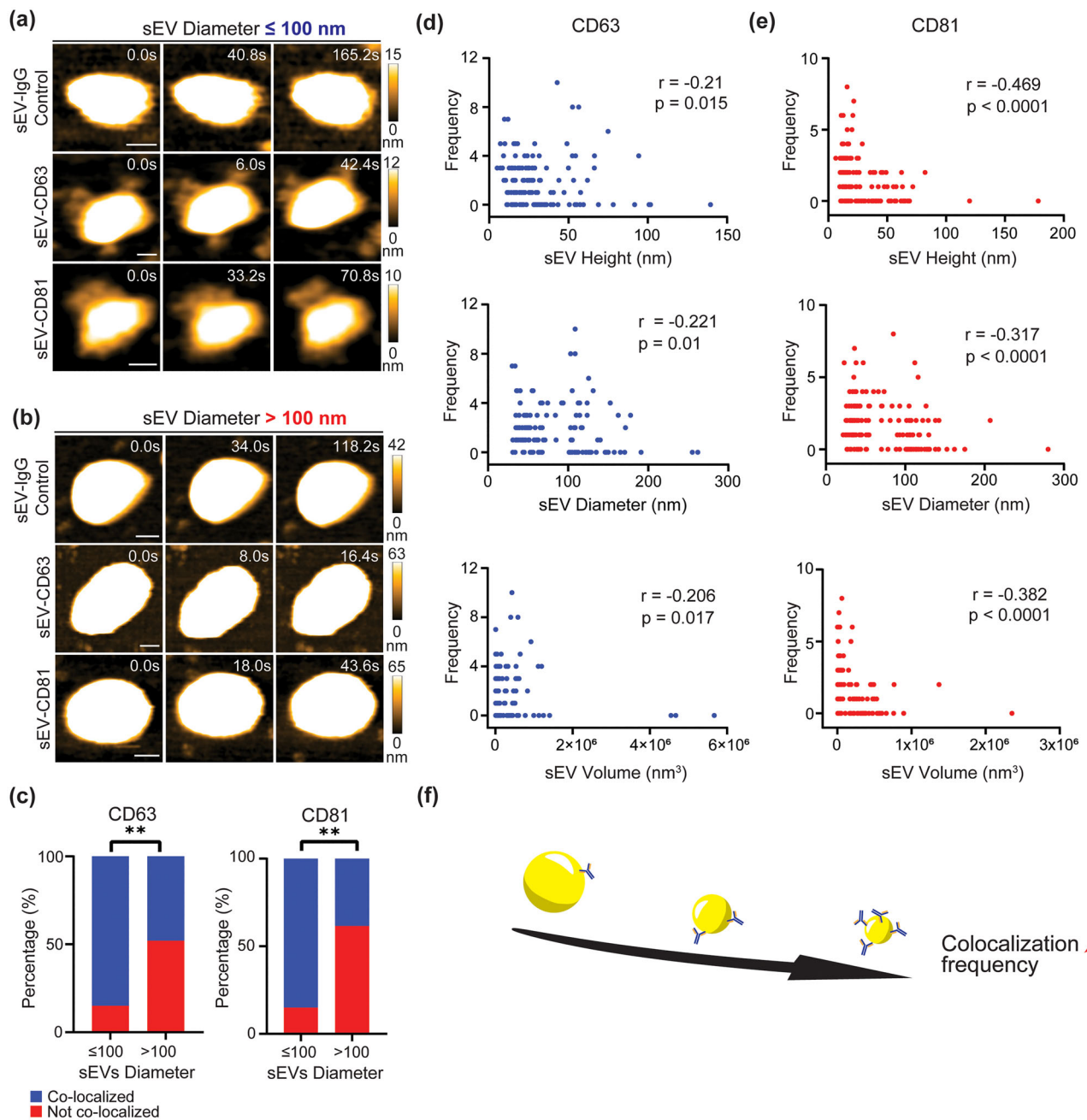
FIGURE 4 | Characterisation of exosome marker-enriched and exosome marker-depleted sEVs at single sEV level. (a and b) HS-AFM image sequences show the interaction between antibodies and $sEV_{d \leq 100\,nm}$ (a) or $sEV_{d > 100\,nm}$ (b). $sEV_{d \leq 100\,nm}$ were found co-localised with anti-tetraspanin antibodies (CD63 and CD81) but not with IgG[control]. (b) Intriguingly, IgG[CD63] and IgG[CD81] rarely co-localised with $sEV_{d > 100\,nm}$ compared with that on $sEV_{d \leq 100\,nm}$ (scale bar, $sEV_{d \leq 100\,nm}$, 20 nm; $sEV_{d > 100\,nm}$, 50 nm). (c) Quantitative analysis revealed the co-localisation percentage of anti-tetraspanin antibodies with $sEV_{d \leq 100\,nm}$ were significantly greater than that with $sEV_{d > 100\,nm}$ (Chi-square test, ** p value < 0.01). (d and e) Correlation analysis suggested that the interaction between sEV and IgG[CD63] or IgG[CD81] was significantly negatively correlated with height, diameter and volume of sEV (Spearman's correlation test). (f) A schematic diagram illustrates that the co-localisation frequency of anti-exosome markers increases as sEV size decreases.

Combining HS-AFM with other methodologies can advance the development of therapeutic strategies for sEV-related diseases. Precise regulation of sEV biogenesis pathways can improve treatment efficacy while minimising potential adverse effects. Our HS-AFM nano-imaging offers a promising approach to optimise laboratory procedures for sEV detection, accelerate research on sEV biogenesis mechanisms, clarify disease mechanisms related to sEVs, and aid in developing relevant diagnostic methods.

Our label-free HS-AFM videography shows the potential for rapid, real-time surface marker profiling of sEVs. This technique may offer a more efficient method for differentiating distinct sEV subpopulations, which is beneficial for exosome isolation and exosomal cargo investigation. In addition, functionalised cantilevers such as macrocyclic peptide-conjugated cantilevers (Puppulin et al. 2021) can be used in HS-AFM for molecular recognition imaging (MRI) to rapidly recognise surface markers
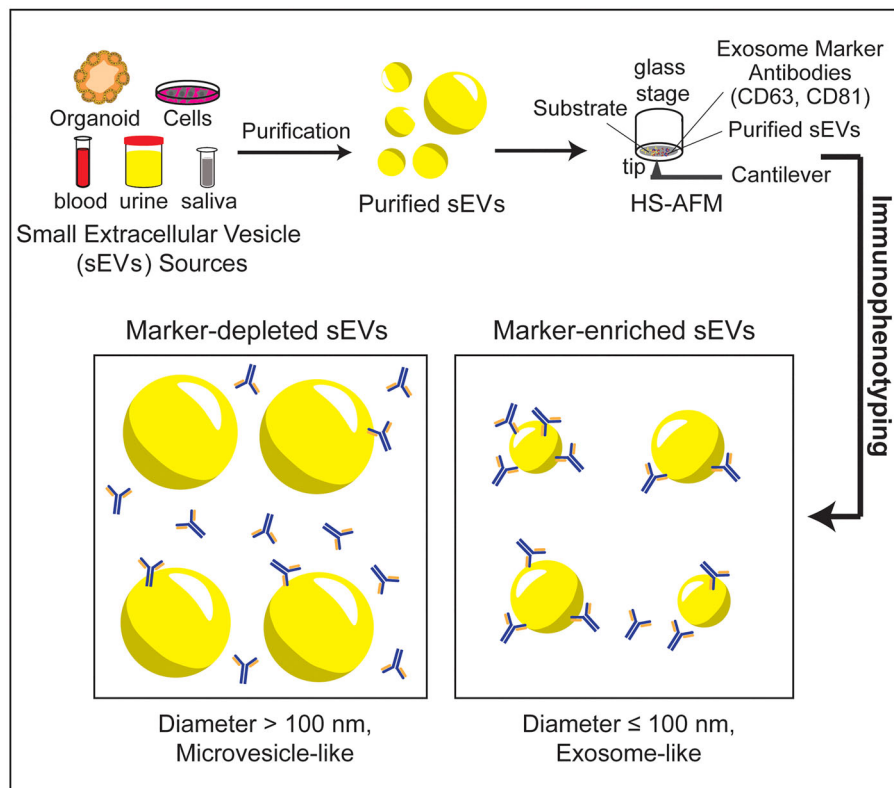
FIGURE 5 | Future prospect of HS-AFM-based nanoscopic immunophenotyping for sEVs isolated from different sources including organoids, cultured cells and clinical samples.

expressed on sEVs. Broadly, HS-AFM videography, together with standard AFM—used for investigating the mechanical properties of sEVs, determining the antibody binding affinity, and performing MRI—can expedite research on sEV biogenesis mechanisms and help elucidate the underlying mechanisms of sEV-associated disorders. HS-AFM holds promise for the development of diagnostic tools related to sEVs. Furthermore, an ultra-wide scanner is available to enhance the productivity of nanoscopic profiling of sEVs (Marchesi et al. 2021). However, certain limitations need to be addressed. For instance, HS-AFM is not yet a high-throughput tool for analysing large batches of clinical sEVs samples. While HS-AFM can rapidly scan numerous sEVs, a sufficient number of HS-AFM experts are required to analyze the resulting data. Standard immunophenotyping of cells provides comprehensive information by detecting multiple surface markers in a single flow cytometry run whereas HS-AFM is currently limited to detecting a single surface marker at a time.

5 | Conclusion

In summary, we demonstrated a nanoscopic profiling technique for sEV using surface exosome marker antibodies and HS-AFM. Our data from nanoscopic videography suggested that the single-step label-free HS-AFM videography can effectively determine the presence or absence of specific surface markers on sEVs. Our study provides a foundation for the future development of nanoscopic immunophenotyping of sEVs using HS-AFM in basic research to elucidate intracellular origins of sEV, sEV-based biomarkers and more (Figure 5). However, further efforts are needed to refine HS-AFM to meet clinical diagnostics.

Conflicts of Interest

The authors declare no conflicts of interest.

Data Availability Statement

The data that support the findings of this study are available from the corresponding author upon reasonable request.

References

Amyot, R., and H. Flechsig. 2020. "BioAFMviewer: An Interactive Interface for Simulated AFM Scanning of Biomolecular Structures and Dynamics." *Plos Computational Biology* 16: e1008444.

Ando, T.. 2012. "High-Speed Atomic Force Microscopy Coming of Age." *Nanotechnology* 23: 062001.

Ando, T., S. Fukuda, K. X. Ngo, and H. Flechsig. 2023. "High-Speed Atomic Force Microscopy for Filming Protein Molecules in Dynamic Action." *Annual Review of Biophysics* 53: 19–39.

Ando, T., T. Uchihashi, N. Kodera, et al. 2007. "High-Speed Atomic Force Microscopy for Observing Dynamic Biomolecular Processes." *Journal of Molecular Recognition* 20: 448–458.

Bongini, L., D. Fanelli, F. Piazza, P. De Los Rios, S. Sandin, and U. Skoglund. 2004. "Freezing Immunoglobulins to See Them Move." *Proceedings of the National Academy of Sciences* 101: 6466–6471.

Chargaff, E., and R. West. 1946. "The Biological Significance of the Thromboplastic Protein of Blood." *Journal of Biological Chemistry* 166: 189–197.

Kalluri, R., and V. S. LeBleu. 2020. "The Biology, Function, and Biomedical Applications of Exosomes." *Science* 367: eaau6977.

Kalra, H., C. G. Adda, M. Liem, et al. 2013. "Comparative Proteomics Evaluation of Plasma Exosome Isolation Techniques and Assessment of the Stability of Exosomes in Normal Human Blood Plasma." *Proteomics* 13: 3354–3364.

Kobayashi, H., T. Shiba, T. Yoshida, et al. 2024. "Precise Analysis of Single Small Extracellular Vesicles Using Flow Cytometry." *Scientific Reports* 14: 7465.

Kowal, J., G. Arras, M. Colombo, et al. 2016. "Proteomic Comparison Defines Novel Markers to Characterize Heterogeneous Populations of Extracellular Vesicle Subtypes." *Proceedings of the National Academy of Sciences* 113: E968–77.

Lim, K., M. Hazawa, and R. W. Wong. 2024. "Crafty Mimicry Grants Nuclear Pore Entry to HIV." *Cell Host & Microbe* 32: 441–442.

Lim, K., N. Kodera, H. Wang, et al. 2020. "High-Speed AFM Reveals Molecular Dynamics of Human Influenza A Hemagglutinin and Its Interaction With Exosomes." *Nano Letters* 20: 6320–6328.

Lim, K., G. Nishide, E. S. Sajidah, et al. 2023. "Nanoscopic Assessment of Anti-SARS-CoV-2 Spike Neutralizing Antibody Using High-Speed AFM." *Nano Letters* 23: 619–628.

Lim, K., G. Nishide, T. Yoshida, et al. 2021. "Millisecond Dynamic of SARS-CoV-2 Spike and Its Interaction With ACE2 Receptor and Small Extracellular Vesicles." *Journal of Extracellular Vesicles* 10: e12170.

Lim, K. S., M. S. Mohamed, H. Wang, et al. 2020. "Direct Visualization of Avian Influenza H5N1 Hemagglutinin Precursor and Its Conformational Change by High-Speed Atomic Force Microscopy." *Biochimica et Biophysica Acta (BBA) - General Subjects* 1864: 129313.

Marchesi, A., K. Umeda, T. Komekawa, et al. 2021. "An Ultra-Wide Scanner for Large-Area High-Speed Atomic Force Microscopy With Megapixel Resolution." *Scientific Reports* 11: 13003.

Meldolesi, J. 2018. "Exosomes and Ectosomes in Intercellular Communication." *Current Biology* 28: R435–R444.

Mohamed, M. S., M. Hazawa, A. Kobayashi, et al. 2020. "Spatiotemporally Tracking of Nano-Biofilaments Inside the Nuclear Pore Complex Core." *Biomaterials* 256: 120198.

Mohamed, M. S., A. Kobayashi, A. Taoka, et al. 2017. "High-Speed Atomic Force Microscopy Reveals Loss of Nuclear Pore Resilience as a Dying Code in Colorectal Cancer Cells." *ACS Nano* 11: 5567–5578.

Nakajima, M., and I. Tamai. 2023. "Roles and Application of Extracellular Vesicles Occurring Endogenously and Naturally." *Pharmaceutical Research* 40: 793–794.

Nishide, G., K. Lim, M. S. Mohamed, et al. 2021. "High-Speed Atomic Force Microscopy Reveals Spatiotemporal Dynamics of Histone Protein H2A Involution by DNA Inchworming." *Journal of Physical Chemistry Letters* 12: 3837–3846.

Nishide, G., K. Lim, M. Tamura, et al. 2023. "Nanoscopic Elucidation of Spontaneous Self-Assembly of Severe Acute Respiratory Syndrome Coronavirus 2 (SARS-CoV-2) Open Reading Frame 6 (ORF6) Protein." *Journal of Physical Chemistry Letters* 14: 8385–8396.

Palanisamy, V., S. Sharma, A. Deshpande, H. Zhou, J. Gimzewski, and D. T. Wong. 2020. "Nanostructural and Transcriptomic Analyses of Human Saliva Derived Exosomes." *PLoS ONE* 5: e8577.

Parisse, P., I., Rago, L. Ulloa Severino, et al. 2017. "Atomic Force Microscopy Analysis of Extracellular Vesicles." *European Biophysics Journal* 46: 813–820.

Preiner, J., N. Kodera, J. Tang, et al. 2014. "IgGs are Made for Walking on Bacterial and Viral Surfaces." *Nature Communications* 5: 4394.

Puppulin, L., D. Kanayama, N. Terasaka, et al. 2021. "Macrocyclic Peptide-Conjugated Tip for Fast and Selective Molecular Recognition Imaging by High-Speed Atomic Force Microscopy." *ACS Applied Materials & Interfaces* 13: 54817–54829.

Qiu, Y., E. S. Sajidah, S. Kondo, et al. 2024. "An Efficient Method for Isolating and Purifying Nuclei From Mice Brain for Single-Molecule Imaging Using High-Speed Atomic Force Microscopy." *Cells* 13, no. 3: 279.

Read, J., A. Ingram, H. A. Al Saleh, et al. 2017. "Nuclear Transportation of Exogenous Epidermal Growth Factor Receptor and Androgen Receptor via Extracellular Vesicles." *European Journal of Cancer* 70: 62–74.

Sajidah, E. S., K. Lim, M. Hazawa, and R. W. Wong. 2024. "Nanoimaging of SARS-CoV-2 Viral Invasion Toward the Nucleus and Genome." *Cell Reports Physical Science* 5: 102111.

Sajidah, E. S., K. Lim, T. Yamano, et al. 2022. "Spatiotemporal Tracking of Small Extracellular Vesicle Nanotopology in Response to Physicochemical Stresses Revealed by HS-AFM." *Journal of Extracellular Vesicles* 11: e12275.

Seltmann, K., B. Hettich, S. Abele, et al. 2024. "Transport of CLCA2 to the Nucleus by Extracellular Vesicles Controls Keratinocyte Survival and Migration." *Journal of Extracellular Vesicles* 13: e12430.

Sharma, S., H. I. Rasool, V. Palanisamy, et al. 2010. "Structural-Mechanical Characterization of Nanoparticle Exosomes in Human Saliva, Using Correlative AFM, FESEM, and Force Spectroscopy." *ACS Nano* 4: 1921–1926.

Strasser, J., R. N. de Jong, F. J. Beurskens, et al. 2019. "Unraveling the Macromolecular Pathways of IgG Oligomerization and Complement Activation on Antigenic Surfaces." *Nano Letters* 19: 4787–4796.

Strasser, J., R. N. de Jong, F. J. Beurskens, et al. 2020. "Weak Fragment Crystallizable (Fc) Domain Interactions Drive the Dynamic Assembly of IgG Oligomers Upon Antigen Recognition." *ACS Nano* 14: 2739–2750.

Tauro, B. J., D. W. Greening, R. A. Mathias, et al. 2012. "Comparison of Ultracentrifugation, Density Gradient Separation, and Immunoaffinity Capture Methods for Isolating Human Colon Cancer Cell Line LIM1863-Derived Exosomes." *Methods (San Diego, Calif.)* 56: 293–304.

Théry, C., K. W. Witwer, E. Aikawa, et al. 2018. "Minimal Information for Studies of Extracellular Vesicles 2018 (MISEV2018): A Position Statement of the International Society for Extracellular Vesicles and Update of the MISEV2014 Guidelines." *Journal of Extracellular Vesicles* 7: 1535750.

Umeda, K., S. J. McArthur, and N. Kodera. 2023. "Spatiotemporal Resolution in High-Speed Atomic Force Microscopy for Studying Biological Macromolecules in Action." *Microscopy (Oxf)* 72: 151–161.

van Niel, G., D. R. F. Carter, A. Clayton, D. W. Lambert, G. Raposo, and P. Vader. 2022. "Challenges and Directions in Studying Cell-Cell Communication by Extracellular Vesicles." *Nature Reviews Molecular Cell Biology* 23: 369–382.

van Niel, G., G. D'Angelo, and G. Raposo. 2018. "Shedding Light on the Cell Biology of Extracellular Vesicles." *Nature Reviews Molecular Cell Biology* 19: 213–228.

Wang, Z., X. Zhou, Q. Kong, et al. 2024. "Extracellular Vesicle Preparation and Analysis: A State-of-the-Art Review." *Advancement of Science (Weinh)* 11: e2401069.

Welsh, J. A., D. C. I. Goberdhan, L. O'Driscoll, et al. 2024. "Minimal Information for Studies of Extracellular Vesicles (MISEV2023): From Basic to Advanced Approaches." *Journal of Extracellular Vesicles* 13: e12404.

Wolf, P. 1967. "The Nature and Significance of Platelet Products in Human Plasma." *British Journal of Haematology* 13: 269–288.

Wong, R. W. 2015. "Nuclear Pore Complex: From Structural View to Chemical Tools." *Chemistry & Biology* 22: 1285–1287.

Yáñez-Mó, M., P. R. Siljander, Z. Andreu, et al. 2015. "Biological Properties of Extracellular Vesicles and Their Physiological Functions." *Journal of Extracellular Vesicles* 4: 27066.

Yim, K. H. W., O. Krzyzaniak, A. Al Hrout, B. Peacock, and R. Chahwan. 2023. "Assessing Extracellular Vesicles in Human Biofluids Using Flow-Based Analyzers." *Advanced Healthcare Materials* 12: e2301706.

Yoshida, T., K. Goto, A. Kodama, D. Bolidong, T. Seto, and R. Hanayama. 2024. "Extracellular Vesicles Promote Silica Nanoparticle Aggregation That Inhibits Silica-Induced Cytotoxicity." *Archives of Biochemistry and Biophysics* 755: 109964.

Yurtsever, A., T. Yoshida, A. Badami Behjat, Y. Araki, R. Hanayama, and T. Fukuma. 2021. "Structural and Mechanical Characteristics of Exosomes From Osteosarcoma Cells Explored by 3D-Atomic Force Microscopy." *Nanoscale* 13: 6661–6677.

Zhang, H., D. Freitas, H. S. Kim, et al. 2018. "Identification of Distinct Nanoparticles and Subsets of Extracellular Vesicles by Asymmetric Flow Field-Flow Fractionation." *Nature Cell Biology* 20: 332–343.

Zhang, P., X. Liu, P. Liu, et al. 2020. "Capturing Transient Antibody Conformations With DNA Origami Epitopes." *Nature Communications* 11: 3114.

Supporting Information

Additional supporting information can be found online in the Supporting Information section.